Journal of Materials Chemistry B

Accepted Manuscript

ROYAL SOCIETY OF CHEMISTRY

www.rsc.org/materialsB

Journal Name

RSCPublishing

ARTICLE

Theranostic Nanoscale Coordination Polymers for Magnetic Resonance Imaging and Bisphosphonate Delivery

Cite this: DOI: 10.1039/x0xx00000x

Demin Liu,[a] Chunbai He,[a] Christopher Poon,[a] and Wenbin Lin[a,*]

Received 00th January 2012,
Accepted 00th January 2012

DOI: 10.1039/x0xx00000x

www.rsc.org/

Nanoscale coordination polymers (NCPs) are self-assembled from metal ions and organic bridging ligands. The tunable compositions, sizes, and shapes; high drug loadings; ease of surface modification; and intrinsic biodegradability make NCPs great candidates for nanomedicine applications. Here we report the self-assembly of a Mn-bisphosphonate NCP that carries exceptionally high loadings of zoledronate (63±5 wt%) and Mn^{2+} ions (13.3±4 wt%) for potential cancer therapy and magnetic resonance imaging, respectively. The Mn-bisphosphonate NCP was further coated with lipid and pegylated to control the drug release kinetics and functionalized with a targeting group (anisamide) to endow specificity to cancer cells, leading to significantly enhanced cytotoxicity against human breast and pancreatic cancer cells. *In vitro* MR imaging studies demonstrated the efficacy of the Mn-bisphosphonate NCP as an effective T_1 contrast agent and confirmed the targeting capability of anisamide-functionalized NCP. Multifunctional NCPs thus present an excellent platform for designing theranostic nanomaterials for a wide range of biomedical applications.

*Dr. Demin Liu, Dr. Chunbai He, Chris Poon, and Prof. Wenbin Lin**
Department of Chemistry
University of Chicago
929 East 57th Street, Chicago, IL 60637, USA
E-mail: wenbinlin@uchicago.edu

Supporting information for this article is available on the WWW under http://dx.doi.org/10.1002/cmdc.20xxxxxxx.

Introduction

Cancer is major public health threat worldwide, and contributes to approximately one quarter of the total death in the United States.[1] This high mortality is primarily due to the metastasis of primary cancer to other organs before they are diagnosed. Although significant advances have been made in cancer detection, many patients are still diagnosed with cancer at late stages due to the relatively low selectivity and sensitivity of current diagnostic techniques.[2] The major impediments of conventional diagnostic agents, such as chelated Gd^{3+} ions for MRI or radiolabeled biomolecules for positron emission tomography (PET) imaging, are their short blood circulation times and nonspecific biodistributions. Small molecule cancer chemotherapeutics also suffer from the same unfavorable pharmacokinetics, leading to nonspecific distribution of highly cytotoxic agents to normal tissues. The resulting narrow therapeutic window of chemotherapeutics prevents eradication of cancer in many patients, and the recurrence and metastasis cause cancer to develop resistance to all treatments. In order to overcome these major obstacles in the detection and treatment of cancer, various nanoparticle platforms have been extensively developed for cancer diagnostics and therapy.

Nanoparticles exhibit several potential advantages over conventional agents, including extended circulation half-lives, passive accumulation at tumor sites due to the enhanced permeability and retention (EPR) effect, active targeting to cancer cells, and avoidance of multidrug resistance.[3-8] Among the various nano-platforms developed so far, theranostic nanoparticles have emerged as a next-generation nanocarrier system to enable both diagnostic and therapeutic functions in the past decade.[9] Theranostic nanoparticles can assist in tracking the absorption, distribution, metabolism, and excretion of nanoparticles *in vivo*, provide a better understanding of the pharmacokinetics of the drug delivery system, identify intracellular targets, improve tumor targeting capability, and finally enable accurate and effective detection and treatment of cancer at an early stage.[10-12]

Among many diagnostic techniques, magnetic resonance imaging (MRI) is a powerful imaging modality due to its ability to provide high spatial resolution and tissue penetration without radioactivity involved in the procedure.[13,14] However, the intrinsic sensitivity of MRI is relatively low, and the widely used small molecule contrast agents have short blood circulation times and non-specific biodistribution profiles. As a result, a relatively high dose of contrast agents is required for adequate contrast enhancement in MR imaging.[15,16] Paramagnetic and superparamagnetic nanoparticles have recently emerged as promising MR contrast agents owing to their ability to carry large payloads of magnetic centers.[17-20] For instance, superparamagnetic ferrite nanoparticles with an extraordinary ability to shorten transverse relaxation times (T_2) have been demonstrated to be effective MRI contrast agents.[21,22] However, this negative contrast enhancement can generate false positives and is difficult to implement in clinical settings. In order to overcome this drawback, Gd^{3+} based nanoparticulate contrast agents capable of shortening longitudinal relaxation times (T_1) have recently been developed.[18,23-26] These nanoparticles have been shown to be superior to commercially available Gd^{3+} complexes in terms of contrast enhancement. However, the potential leaching of Gd^{3+} ions, which are responsible for the potentially fatal condition known as nephrogenic systemic fibrosis (NSF) in patients with severely impaired renal function, presents a major problem for further development of Gd-based nanoparticulate contrast agents.[23,27] Mn^{2+}-based nanoparticles present an interesting alternative due to the lower toxicity of Mn^{2+} ions and their ability to provide more efficient T_1-weighted contrast enhancement when binding to intracellular proteins.[28-30]

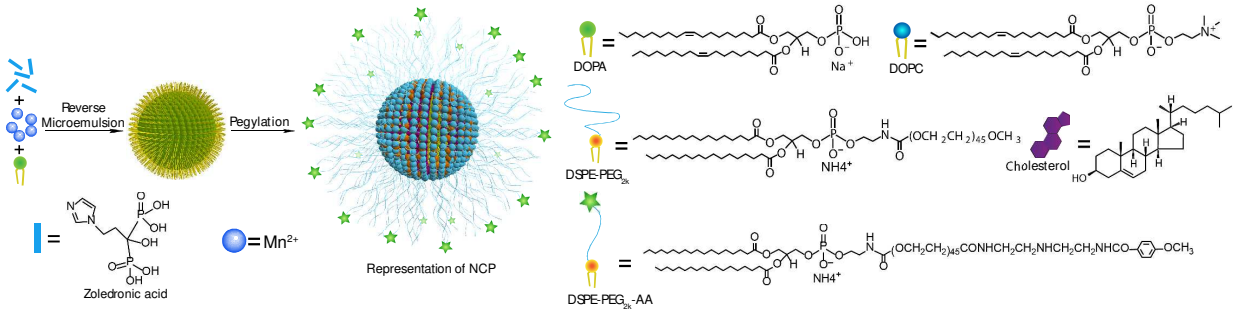

Scheme 1. Schematic showing the general procedure for the self-assembly of NCPs with lipid and PEG coating.

Nitrogen-containing bisphosphonates (N-BPs) effectively inhibit osteoclast-mediated bone resorption and are integral in the treatment of benign and malignant bone diseases. Recently, they are found to have antitumor effect, as evidenced by reduced proliferation and viability of cancer cells *in vitro* and reduced skeletal tumor burden and slower progression of bone lesions in animal models.[31-36] N-BPs are shown to inhibit farnesyl pyrophosphate synthase (FPPS), a key enzyme in the mevalonate pathway involved in the synthesis of geranylgeranyl pyrophosphate (GGPP). At the

same time, a new cytotoxic adenosine triphosphate (ATP) analog called triphosphoric acid 1-adenosin-5'-yl ester 3-(3-methylbut-3-enyl) ester (ApppI) is formed during the process. ApppI can induce apoptosis similar to adenosine 5′-(β,γ-dichloromethylene) triphosphate (AppCC12p). In addition, N-BPs also inhibit the adhesion of cancer cells to extracellular matrix (ECM) proteins and the process of cancer cell invasion and metastasis. Furthermore, antiangiogenic effects of N-BPs have been demonstrated both *in vitro* and *in vivo*.[33,37] Zoledronic acid, one of the most effective N-BPs, has been shown to be beneficial for breast cancer patients in several Phase III studies in the adjuvant setting: it not only reduces the fracture risk but also provides significant survival benefit over placebo and no treatment.[38,39] However, the clinical application of bisphosphonates as anticancer therapeutics is limited by their unfavorable pharmacokinetics as the majority of the injected drugs either bind to the bones or are quickly cleared through renal filtration.

Several nano-platforms have been examined for bisphosphonate delivery to certain tumor cells, but relatively low drug loadings were achieved in these studies.[40-43] Our group has previously shown that nanoscale metal-organic frameworks (NMOFs) or nanoscale coordination polymers (NCPs) can serve as effective nanocarriers for delivery of chemotherapeutic agents[44,45,46] and contrast agents for optical imaging,[47] X-ray computed tomography (CT) imaging[48] and MRI imaging.[49,50] Extremely high cargo loadings were realized in these studies. We hypothesize that high compositional tunability of NCPs should arrow us to integrate imaging and therapy into one single formulation for cancer specific diagnosis and chemotherapy. In this paper, we report the synthesis and characterization of multifunctional NCPs carrying exceptionally high loadings of anticancer agent, zoledronate, and T_1-weighted MRI contrast agent, Mn^{2+} ions, for *in vitro* theranostic applications (Scheme 1). The Mn-bisphosphonate NCP was further pegylated to control the drug release kinetics and functionalized with a targeting group (anisamide) to endow specificity to cancer cells, leading to significantly enhanced cytotoxicity against human breast and pancreatic cancer cells. *In vitro* MR imaging studies demonstrated the efficacy of the Mn-bisphosphonate NCP as an effective T_1 contrast agent and confirmed the targeting capability of anisamide-functionalized NCP. Our work has thus established a novel, tunable platform for designing multifunctional nanomaterials for theranostic applications.

Results and Discussion

Synthesis and characterization of NCPs.

The Mn-bisphosphonate NCP (1) was synthesized by a microwave reaction of zoledronic acid and $MnCl_2$ in the presence of 1,2-dioleoyl-sn-glycero-3-phosphate sodium salt (DOPA) in dimethylformamide (DMF)/H_2O at 140 °C for 10 min. Amorphous particles of **1** were isolated via centrifugation and washed with cyclohexane and ethanol. Transmission electron microscopy (TEM) images of **1** (Figure 1a) demonstrated the formation of nanoparticles of fairly uniform shape. The particle diameter was determined to be 55.8±4.2 nm by dynamic light scattering (DLS). Zoledronic acid loading was determined by ultraviolet-visible (UV-Vis) spectroscopy to be 63±5 wt%. The as-synthesized particles of **1** decompose rapidly in 5 mM phosphate buffered saline (PBS) pH=7.4 as shown in Figure 2a with a half-life ($t_{1/2}$) less than 1 h. In order to improve the drug release kinetics in biologically relevant media and render them biocompatibility, we coated these particles with a lipid/lipid-peg layer.[51-54] The lipid coated and pegylated **1** (**1**@peg) was obtained by following previously reported procedures.[45] Briefly, a THF solution of 1,2-dioleoyl-sn-glycero-3-phosphocholine (DOPC), cholesterol (1:1 molar ratio), 1,2-distearoyl-sn-glycero-3-phosphoethanolamine-N-[amino(polyethylene glycol)2000] (DSPE-PEG_{2k} 20 mol%) and nanoparticles was added to 500 uL of 30% (v/v) EtOH/H_2O at 50 °C. THF was evaporated and the solution was allowed to cool to room temperature before use. Nanoparticles after lipid coating and pegylation are about 20 nm bigger than bare particles while possessing the similar morphology (Figure 1c), which is due to the single lipid layer and hydrodynamic diameter of PEG_{2k} added to the surface of **1**. As shown in Table 1, the diameter of **1**@peg is 75.8±8.1nm and the ζ potenital after pegylation is around neutral in PBS buffer. Drug loading after pegylation was determined to be 42±7 wt%. The stability of **1**@peg was first evaluated "*in vitro*" in PBS buffer with bovine serum albumin (BSA) at a concentration over 5 mg/ml at 37 °C. As shown in Figure 2b, particle sizes were not altered over a 12 h period, showing excellent colloidal stability of these particles. The enhanced stability of **1**@peg was further confirmed by the release profile experiment which gave a $t_{1/2}$ of 98 h and approximately 65 % drug release in 140 h in 5 mM PBS at 37 °C.

Table 1. Characterization data for **1** and related particles.

NCPs	Number-Average diameter (nm)	PDI	ζ Potential (mV)	Drug loading (wt%)	Mn loading (wt%)	Zoledronate to Mn molar ratio	MCF-7 IC_{50}/ μM	AsPC-1 IC_{50}/ μM
1	55.8±4.2	0.14	NP	63±5	13.3±4	0.96:1	>15	>40
1@peg	75.8±8.1	0.12	-0.4±1.1	42±7	10.1±2	0.85:1	6.4±1.5	24±5.0
1@peg-AA	78.6±5.4	0.14	-1.0±0.7	40±4	9.7±2	0.84:1	2.0±0.9	13±1.4

Journal Name

RSCPublishing

ARTICLE

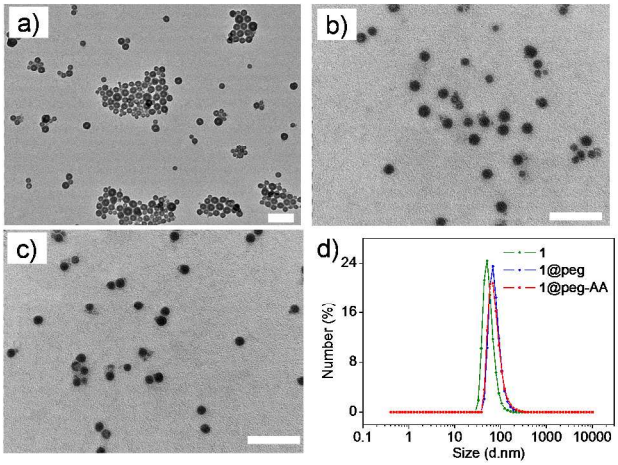

Figure 1. TEM images of a) **1**. b) **1**@peg. c) **1**@peg-AA. d) Size distribution of **1** and related particles measured by dynamic light scattering. Scale bars = 200 nm.

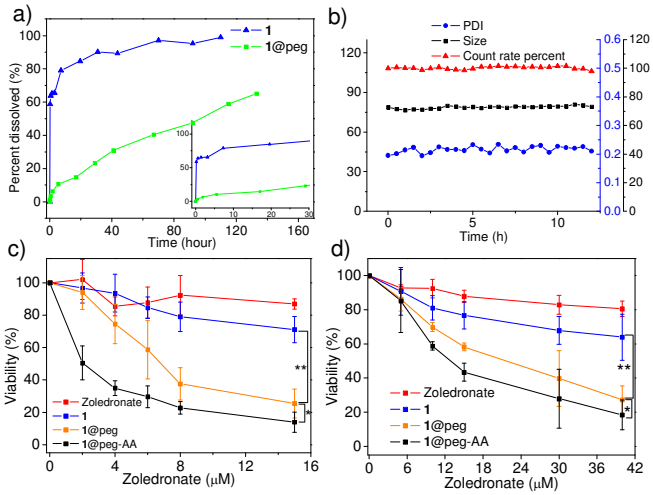

Figure 2. a) Release profiles of **1** and **1**@peg in 5 mM PBS buffer at 37 °C. b) Stability test of **1**@peg in PBS buffer with BSA at 37 °C. *In vitro* cytotoxicity assays of **1** and related particles against MCF-7 (c) and AsPC-1(d). Error bars represent one standard deviation.*p<0.05, **p<0.01, ***p<0.001.

In vitro cytotoxicity and confocal microscopy studies of anisamide-targted NCPs.

Anisamide (AA) is a small molecule which has been shown to target σ receptors that are overexpressed by many cancer cells, including MCF-7 human breast adenocarcinoma cells and AsPC-1 human pancreatic cancer cells.[55-57] 10 mol% of DSPE-PEG_{2K}-AA was incorporated into the lipid formulation, and the resulting **1**@peg-AA showed similar morphology (Figure 1b), size, drug loadings, and ζ potenitals as their undoped counterparts (Table 1). We first performed *in vitro* cytotoxicity assays on MCF-7 cells (Figure 2c). The free drug and as-synthesized **1** did not lead to any appreciable cell death, as a result of their inability to enter the cells. However, **1**@peg showed significantly higher potency with an IC_{50} (50 % inhibitory concentration) value of 6.4±1.5 μM compared to the free zoledronic acid group. A significantly lower IC_{50} value was observed in cells treated with **1**@peg-AA (2.0±0.9 μM) when compared to the value in cells incubated with non-targeted particles. Thus, pegylated and AA-targeted NCPs can be effectively internalized by cells via σ receptor-mediated endocytosis. We also performed *in vitro* cytotoxicity assays on AsPC-1 cells (Figure 2d). An IC_{50} value of 24±5.0 μM for **1**@peg and a significantly lower value of 13±1.4 μM for **1**@peg-AA was obtained after 48 h incubation. We performed confocal laser scanning microscopy (CLSM) to study cell uptake pathways. As shown in Figure 3, the co-localizaiton of red fluorescence from **1'**@peg and **1'**@peg-AA (see below) and green fluorescence from lysotracker green confirmed that particles were internalized via endocytosis pathways.

The targeting capability of NCPs was further supported by CLSM studies. To visualize particles inside cells, 2 wt% of chlorin e6 was doped into **1** for imaging purpose (denoted as **1'**, SI). **1'** adopted a spherical shape with a diameter of 48.4±3.2 nm. The lipid coating and pegylation was performed in the same way as **1** and the diameter of **1'**@peg was determined by DLS to be 65±7 nm (Figure 1d). The cells were also stained with Annexin V-FITC apoptosis marker. As shown in Figure 4, significant fluorescence signal from FITC (green) and chlorin e6 (red) was observed in the confocal images of MCF-7 cells incubated with **1'**@peg-AA. In contrast, much weaker signals were observed for MCF-7 cells incubated with **1'**@peg. This observation indicates that AA targeting enhances particle uptake to lead to increased levels of apoptosis in cells treated with **1'**@peg-AA.

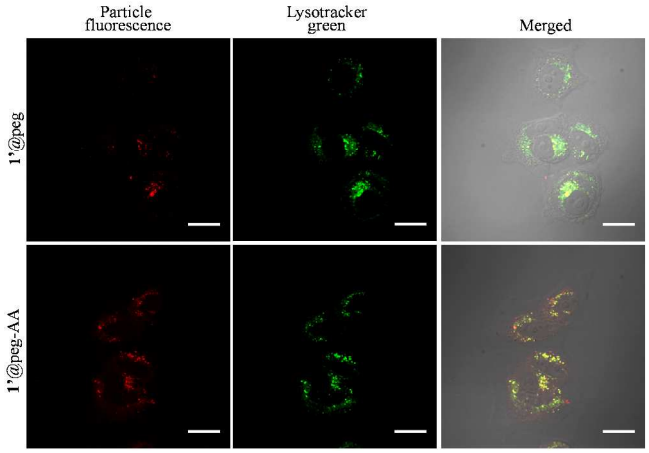

Figure 3. CLSM images of MCF-7 cells incubated with **1**'@peg and **1**'@peg-AA. Channels are: chlorin e6 from the particles (red) and lysotracker (green). Scale bars are 20 μm.

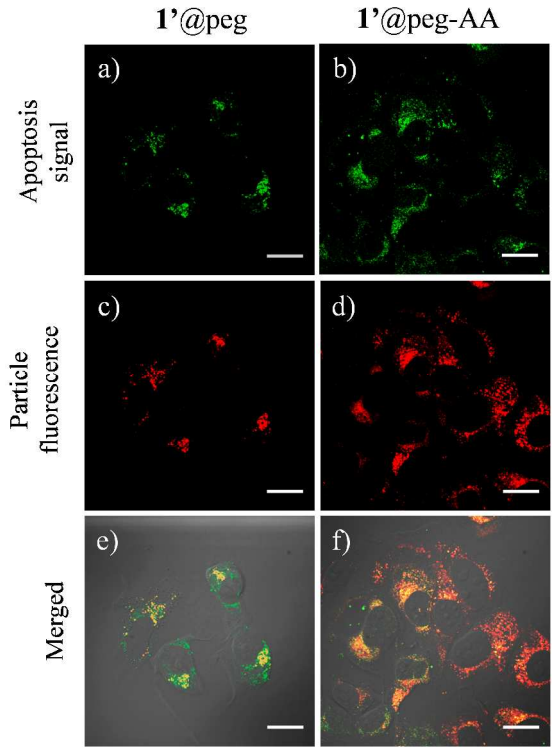

Figure 4. CLSM images of MCF-7 cells incubated with **1**'@peg (a, c, e) and **1**'@peg-AA (b, d, f). Channels are: Annexin V FITC conjugate early apoptosis stain (green), and chlorin e6 from the particles (red). Scale bares are 20 μm.

We also quantified cell apoptosis using flow cytometry. In line with the cytotoxicity assays and CLSM results, no apoptosis was observed for free zoledronic acid group after 24 h incubation. In contrast, the total apoptotic cell percentage (including early and late apoptosis) in MCF-7 cells incubated with **1**@peg and **1**@peg-AA was determined to be 69.6% and 86.0 %, respectively, indicating that anisamide-targeted NCP was more potent and effective in inducing cell apoptosis (Figure 5).

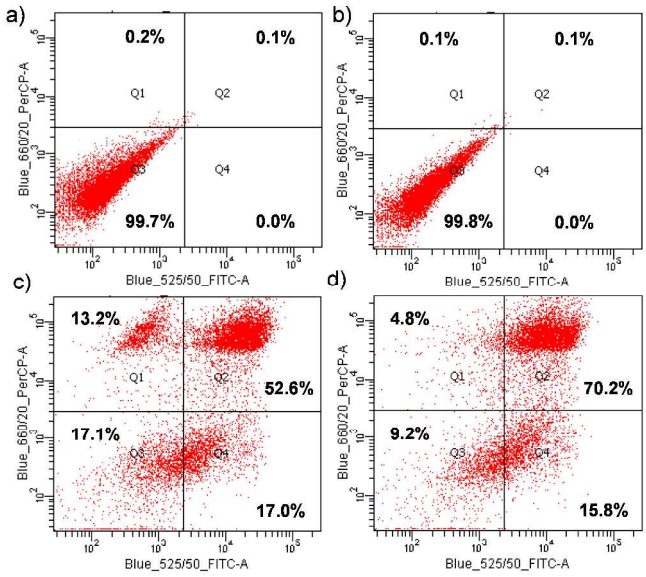

Figure 5. Annexin V/PI analysis of MCF-7 cells after incubation with saline control (a), free zoledronic acid (b), **1**'@peg (c) and **1**'@peg-AA (d) for 24h. The Q1-Q4 quadrants represent necrosis, late apoptotic, healthy, and early apoptotic cells, respectively. The percentage of cells in each quadrant was shown on the graphs.

Competitive binding assay also confirmed the targeting ability of anisamide-functionalized NCP. Pre-incubation of MCF-7 cells with DSPE-PEG-AA (1, 5, and 10 mM) significantly reduced the uptake of **1**@peg-AA (P=0.005, 0.002, and 0.001) but not **1**@peg when compared to those without pre-incubation with the anisamide ligand (Table 2).

Table 2. Competitive binding assay using DSPE-PEG-AA with the particle uptake (μg NCP/mg cellular protein) expressed as mean±SD.[a]

DSPE-PEG-AA (mM)	0	1	5	10
1@peg	1.63±0.06	1.63±0.12	1.57±0.05	1.60±0.12
1@peg-AA	4.72±0.25	3.16±0.07**	2.14±0.06**	1.87±0.08**

[a]Statistical analysis was performed against 0 mM DSPE-PEG-AA. *p<0.05, **p<0.01, ***p<0.001.

Relaxivity measurement of NCPs and *in vitro* MRI study.

To explore their MR imaging contrast capacity, we first determined the MR relaxivities of **1** and related particles using a 3.0-T MR scanner. Nanoparticles of **1** and **1**@peg were found to have a longitudinal relaxivity (r_1) of 4.66 $mM^{-1}s^{-1}$ and 11.6 $mM^{-1}s^{-1}$ and a transverse relaxivity (r_2) of 22.2 $mM^{-1}s^{-1}$ and 19.7 $mM^{-1}s^{-1}$, respectively (Figure 6). These relaxivity values

are slightly higher than the free $MnCl_2$ (r_1=3.83 and r_2=18.4 $mM^{-1}s^{-1}$), presumably as a result of the reduced tumbling rates of NCPs in aqueous solution. The **1**@peg-AA nanoparticles have an r_1 value of 7.6 and r_2 value of 70.3 $mM^{-1}s^{-1}$. The slight decrease of MR relaxivities of the AA targeted nanoparticles is expected because of the reduced influence of the Mn centers on the surrounding water molecules due to the hydrophobicity of the anisamide moiety on the surface. The r_1 values exhibited by the Mn NCPs are much higher than those reported for many other Mn-based nanomaterials (ranging from 0.1 to 7 $mM^{-1}s^{-1}$ with exception of Mn nanocolloid and Mn doped silicon quantum dots).[58-65] To test the diagnostic capability of **1**, we evaluated the efficacy of **1** as MR contrast agents *in vitro* with MCF-7 cells. As shown in Figure 6e and f, the MCF-7 cells incubated with **1**@peg-AA gave much higher signals in T_1-weighted images than those that were not incubated with any nanoparticles and those that were incubated with the non-targeted particles at the 24 h time point. ICP-MS analysis also confirmed the enhanced uptake of **1**@peg-AA by MCF-7 cells. The Mn^{2+} content was determined to be 99.1±9.3 and 191.3±29.9 μg/g cell for **1**@peg and **1**@peg-AA at 24h time point, respectively. **1**@peg-AA was internalized in a higher proportion than the other samples due to the presence of the anisamide ligand that targets sigma receptor overexpressed by the MCF-7 cells. These data further support the enhanced uptake of **1**@peg-AA by MCF-7 cells to result in higher cytotoxicity. We further estimated the r_1 value of **1** to be ~8 $mM^{-1}s^{-1}$ in MCF-7 cells, confirming the ability of **1** to act as an efficient T_1-weighted MR contrast agent *in vitro*.

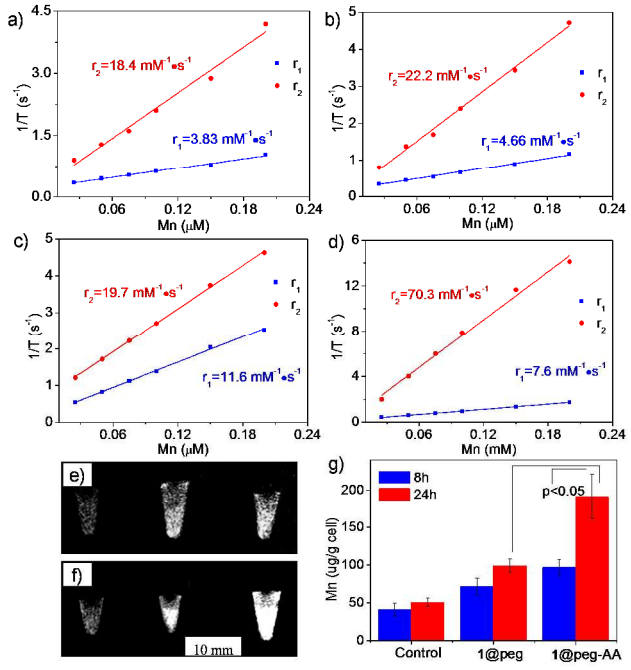

Figure 6. Longitudinal (r_1, squares) and transverse (r_2, circles) MR relaxivity plots of $MnCl_2$ (a), **1** (b), **1**@peg (c), and **1**@peg-AA (d). T_1-weighted images of MCF-7 cell pellets, left: cells incubated without any nanoparticles; middle: cells incubated with **1**@peg; right: cells incubated with **1**@peg-AA at 8 h (e) and 24 h (f) time point. g) Mn uptake study of MCF-7 cells by ICP-MS showing enhanced uptake of anisamide targeted nanoparticles. The r_1 value of **1** in MCF-7 cells was estimated to be ~8 $mM^{-1}s^{-1}$.

Conclusions

We have designed and characterized a theranostic NCP platform that is capable of delivering chemotherapeutic and an MR imaging contrast agent simultaneously to cancer cells with exceptionally high cargo loadings. Surface functionalization with PEG and anisamide-targeted PEG endowed them with physiological stability, biocompatibility and cancer-target specificity. Their ability to induce apoptosis in both human breast and pancreatic cancer cells was demonstrated in the cytotoxicity assays and their MR imaging contrast capability was shown in the *in vitro* MR imaging studies. The tunability of NCPs should allow us to integrate many other therapeutic agents into a single formulation for optimized cancer diagnosis and therapy.

Experimental Section

Synthesis of NCP 1. Zoledronic acid (5 mg, 0.019 mmol), $MnCl2{\cdot}4H_2O$ (10 mg, 0.05 mmol), and 5 mg DOPA were dissolved in a solvent mixture of DMF/H2O (16 mL/3 mL). The resulting solution was sealed in a microwave vessel and placed in the microwave oven with the power set to 800 W and run time set to 2 minutes. After 10 minutes of heating at 140 oC with stirring, the amorphous particles of 1 were isolated via centrifugation at 13000 rpm for 15 min. Before re-dispersing them in THF, the particles were washed once with cyclohexane and twice with EtOH. Approximately 2.3 mg (28 %) particles of 1 were isolated from this procedure.

Lipid coating and pegylation. The lipid coated and pegylated particles were obtained by adding a THF solution of DOPC, cholesterol (1:1molar ratio), DSPE-PEG2k (20 mol%), and 1 to 500 uL of 30% (v/v) EtOH/H2O at 50 oC. THF was evaporated and the solution was allowed to cool to room temperature before use.

Confocal laser scanning microscopy study. Coverslips in 6-well plates were seeded with MCF-7 cells at the density of 105 cells/well. The cells were incubated at 37°C and 5% CO2 for 24 h prior to nanoparticle treatment. Chlorin e6-doped particles of 1 were incubated with MCF-7 cells at 37 °C and 5% CO2 for 24 h. Then, the cells were washed with PBS, fixed with iced 4% paraformaldehyde, and stained with Alexa Fluor 488 conjugated Annexin V (Invitrogen, USA) according to the manufacturer's instructions. The cells were observed using confocal laser scanning microscopy (CLSM, Zeiss LSM710, German) at an excitation wavelength of 405 nm and 488 nm to visualize nanoparticle internalization (red fluorescence) and cell apoptosis (green fluorescence), respectively.

Competitive binding assay. MCF-7 cells were seeded on 24-well plate at 1×105 cells per well and cultured for 24 h. The cells were pre-incubated with 1, 5, or 10 mM of DSPE-PEG-AA for 2 h followed by the addition of 1'@peg and 1'@peg-AA (32 ug/mL). Following a 4-h incubation, cells were washed with PBS three times and then lysed with 0.5% (w/v) sodium dodecyl sulfate (SDS, pH 8.0). The lysate was quantified for Ce6 by fluorimetry (λex/λem=410 nm/660 nm) and protein content by the BCA kit (Promega, USA). Uptake level was expressed as the amount of Ce6 doped nanoparticles associated with 1 mg of cellular protein.

Flow cytometry study. MCF-7 cells were seeded at 1×10^6 cells per well in 6-well plates and further cultured for 24 h. The culture media were replaced by 2 mL of fresh culture media containing 10% FBS. Free zoledronic acid solution, **1**@peg and **1**@peg-AA were added to the cells, respectively, at a zoledronate concentration of 12 μM. Cells incubated with saline served as control. Following incubation for 24 h, the floating and adherent cells were collected by cell scraper and stained with Alexa Fluor 488 annexin V/dead cell apoptosis kit with Alexa Fluor 488 annexin V and PI (Invitrogen, USA) according to the manufacturer's instructions. The apoptosis was examined on a flow cytometer (LSRII Blue, BD, USA).

MRI Studies. MR images were acquired on a Siemens 3T Allegra scanner (Siemens Medical Systems, Erlagen, Germany) with a CP coil. For images acquired on the 3 T scanner, a 3D FLASH sequence was utilized to compute T1 maps with seven different flip angles (2, 5, 10, 20, 30, 40, and 60). Imaging parameters were: FOV=190 x 190 x 64 mm^3, matrix size= 128 x 128 x 32, TR/TE= 40/1.64 ms; total data acquisition time was 30 minutes. A 2-D multiple echo spin echo sequence was used to estimate T2 maps. In total, 32 echoes with an echo spacing of 6.2 ms were obtained. The first echo time was 6.2 ms. TR was 3000 ms. FOV and matrix size were set to 190 x 190 mm^2 and 128 x 128. The slice thickness was 2 mm, and the total data acquisition time was about 6 minutes and 29 seconds. All images were acquired on a Siemens Allegra 3T system.
T_1-weighted MRI relaxivities of **1**, **1**@peg and **1**@peg-AA were measured using 3T MR scanner. Samples of these materials containing different concentrations of Mn^{2+} were prepared to determine the longitudinal (r_1) and transverse (r_2) relaxivities.

Acknowledgements

We thank National Cancer Institute (UO1-CA151455) for funding support and Mr. Shunzhi Wang and Dr. Juan L. Vivero-Escoto for experimental help.

Notes and references

[a]Department of Chemistry, University of Chicago, 929 East 57th Street, Chicago, IL 60637, USA; E-mail: wenbinlin@uchicago.edu

Electronic Supplementary Information (ESI) available: Detailed experimental procedures of *in vitro* assays and MR relaxivity measurements. See DOI: 10.1039/b000000x/

(1) Siegel, R.; Naishadham, D.; Jemal, A. *CA-Cancer J. Clin.* **2013**, *63*, 11.

(2) Choi, K. Y.; Liu, G.; Lee, S.; Chen, X. *Nanoscale* **2012**, *4*, 330.

(3) Bardhan, R.; Lal, S.; Joshi, A.; Halas, N. J. *Acc. Chem. Res.* **2011**, *44*, 936.

(4) Wang, A. Z.; Langer, R. S.; Farokhzad, O. C. *Annu. Rev. Med.* **2011**, *63*, 185.

(5) Lovell, J. F.; Jin, C. S.; Huynh, E.; Jin, H.; Kim, C.; Rubinstein, J. L.; Chan, W. C. W.; Cao, W.; Wang, L. V.; Zheng, G. *Nat. Mater.* **2011**, *10*, 324.

(6) Perrault, S. D.; Chan, W. C. W. *Proc. Natl. Acad. Sci.* **2010**, *107*, 11194.

(7) Cobley, C. M.; Chen, J.; Cho, E. C.; Wang, L. V.; Xia, Y. *Chem. Soc. Rev.* **2011**, *40*, 44.

(8) Yavuz, M. S.; Cheng, Y.; Chen, J.; Cobley, C. M.; Zhang, Q.; Rycenga, M.; Xie, J.; Kim, C.; Song, K. H.; Schwartz, A. G.; Wang, L. V.; Xia, Y. *Nat. Mater.* **2009**, *8*, 935.

(9) Chen, X. *Theranostics* **2011**, *1*, 1.

(10) Perry, J. L.; Herlihy, K. P.; Napier, M. E.; DeSimone, J. M. *Acc. Chem. Res.* **2011**, null.

(11) Shi, J.; Votruba, A. R.; Farokhzad, O. C.; Langer, R. *Nano Lett.* **2010**, *10*, 3223.

(12) Lammers, T.; Aime, S.; Hennink, W. E.; Storm, G.; Kiessling, F. *Acc. Chem. Res.* **2011**, *44*, 1029.

(13) Viswanathan, S.; Kovacs, Z.; Green, K. N.; Ratnakar, S. J.; Sherry, A. D. *Chem. Rev.* **2010**, *110*, 2960.

(14) Jun, Y.-w.; Lee, J.-H.; Cheon, J. *Angew. Chem. Int. Ed.* **2008**, *47*, 5122.

(15) Caravan, P.; Ellison, J. J.; McMurry, T. J.; Lauffer, R. B. *Chem Rev* **1999**, *99*, 2293.

(16) L. Villaraza, A. J.; Bumb, A.; Brechbiel, M. W. *Chem. Rev.* **2010**.

(17) Cheon, J.; Lee, J.-H. *Acc. Chem. Res.* **2008**, *41*, 1630.

(18) Reddy, L. H.; Arias, J. L.; Nicolas, J.; Couvreur, P. *Chem. Rev.* **2012**, *112*, 5818.

(19) Gao, J.; Gu, H.; Xu, B. *Acc. Chem. Res.* **2009**, *42*, 1097.

(20) Huh, Y. M.; Jun, Y. W.; Song, H. T.; Kim, S.; Choi, J. S.; Lee, J. H.; Yoon, S.; Kim, K. S.; Shin, J. S.; Suh, J. S.; Cheon, J. *J. Am. Chem. Soc.* **2005**, *127*, 12387.

(21) Lee, N.; Choi, Y.; Lee, Y.; Park, M.; Moon, W. K.; Choi, S. H.; Hyeon, T. *Nano Lett.* **2012**, *12*, 3127.

(22) Lee, N.; Kim, H.; Choi, S. H.; Park, M.; Kim, D.; Kim, H.-C.; Choi, Y.; Lin, S.; Kim, B. H.; Jung, H. S.; Kim, H.; Park, K. S.; Moon, W. K.; Hyeon, T. *Proc. Natl. Acad. Sci.* **2011**, *108*, 2662.

(23) Vivero-Escoto, J. L.; Taylor-Pashow, K. M. L.; Huxford, R. C.; Della Rocca, J.; Okoruwa, C.; An, H.; Lin, W.; Lin, W. *Small* **2011**, *7*, 3519.

(24) L. Villaraza, A. J.; Bumb, A.; Brechbiel, M. W. *Chem. Rev.* **2010**, *110*, 2921.

(25) Yang, H.; Santra, S.; Walter, G. A.; Holloway, P. H. *Adv. Mater.* **2006**, *18*, 2890.

(26) Plush, S. E.; Woods, M.; Zhou, Y.-F.; Kadali, S. B.; Wong, M. S.; Sherry, A. D. *J. Am. Chem. Soc.* **2009**, *131*, 15918.

(27) Lin, W. B.; Hyeon, T.; Lanza, G. M.; Zhang, M. Q.; Meade, T. J. *MRS Bull.* **2009**, *34*, 441.

(28) Koretsky, A. P.; Silva, A. C. *NMR Biomed.* **2004**, *17*, 527.

(29) Elizondo, G.; Fretz, C. J.; Stark, D. D.; Rocklage, S. M.; Quay, S. C.; Worah, D.; Tsan, Y.-M.; Chen, M. C.-M.; Ferrucci, J. T. *Radiology* **1991**, *178*, 73.

(30) Pan, D.; Schmieder, A. H.; Wickline, S. A.; Lanza, G. M. *Tetrahedron* **2011**, *67*, 8431.

(31) Zhang, Y.; Cao, R.; Yin, F.; Hudock, M. P.; Guo, R.-T.; Krysiak, K.; Mukherjee, S.; Gao, Y.-G.; Robinson, H.; Song, Y.; No, J. H.; Bergan, K.; Leon, A.; Cass, L.; Goddard, A.; Chang, T.-K.; Lin, F.-Y.; Beek, E. V.; Papapoulos, S.; Wang, A. H. J.; Kubo, T.; Ochi, M.; Mukkamala, D.; Oldfield, E. *J. Am. Chem. Soc.* **2009**, *131*, 5153.

(32) El Moll, H.; Zhu, W.; Oldfield, E.; Rodriguez-Albelo, L. M.; Mialane, P.; Marrot, J. r. m.; Vila, N.; Mbomekall √ ©, I. M.; Rivi √ ®re, E.; Duboc, C.; Dolbecq, A. *Inorg. Chem.* **2012**, *51*, 7921.

(33) Green, J. R. *Oncologist* **2004**, *9*, 3.

(34) Morgan, G.; Lipton, A. *Semin. Oncol.* **2010**, *37, Supplement 2*, S30.

(35) Boissier, S.; Ferreras, M.; Peyruchaud, O.; Magnetto, S.; Ebetino, F. H.; Colombel, M.; Delmas, P.; Delaissé, J.-M.; Clézardin, P. *Cancer Res.* **2000**, *60*, 2949.

(36) Compain, J.-D.; Mialane, P.; Marrot, J.; Sécheresse, F.; Zhu, W.; Oldfield , E.; Dolbecq, A. *Chem. Eur. J.* **2010**, *16*, 13741.

(37) Lipton, A. *Expert Opin. Pharmacother.* **2011**, *12*, 749.

(38) Valachis, A.; Polyzos, N. P.; Coleman, R. E.; Gnant, M.; Eidtmann, H.; Brufsky, A. M.; Aft, R.; Tevaarwerk, A. J.; Swenson, K.; Lind, P.; Mauri, D. *The Oncologist* **2013**, *18*, 353.

(39) Saad, F. *Future Oncol.* **2005**, *1*, 149.

(40) Josse, S.; Faucheux, C.; Soueidan, A.; Grimandi, G.; Massiot, D.; Alonso, B.; Janvier, P.; Laïb, S.; Gauthier, O.; Daculsi, G.; Guicheux, J.; Bujoli, B.; Bouler, J. M. *Adv. Mater.* **2004**, *16*, 1423.

(41) Salzano, G.; Marra, M.; Porru, M.; Zappavigna, S.; Abbruzzese, A.; La Rotonda, M. I.; Leonetti, C.; Caraglia, M.; De Rosa, G. *Int. J. Pharm.* **2011**, *403*, 292.

(42) Marra, M.; Salzano, G.; Leonetti, C.; Tassone, P.; Scarsella, M.; Zappavigna, S.; Calimeri, T.; Franco, R.; Liguori, G.; Cigliana, G.; Ascani, R.; La Rotonda, M. I.; Abbruzzese, A.; Tagliaferri, P.; Caraglia, M.; De Rosa, G. *Nanomed. Nanotechnol. Biol. Med.* **2011**, *7*, 955.

(43) Shmeeda, H.; Amitay, Y.; Tzemach, D.; Gorin, J.; Gabizon, A. *J. Controlled Release* **2013**, *167*, 265.

(44) Rieter, W. J.; Pott, K. M.; Taylor, K. M. L.; Lin, W. *J. Am. Chem. Soc.* **2008**, *130*, 11584.

(45) Huxford-Phillips, R. C.; Russell, S. R.; Liu, D.; Lin, W. *RSC Adv.* **2013**, *3*, 14438.

(46) Huxford, R. C.; deKrafft, K. E.; Boyle, W. S.; Liu, D.; Lin, W. *Chem. Sci.* **2012**, *3*, 198.

(47) Liu, D.; Huxford, R. C.; Lin, W. *Angew. Chem. Int. Ed.* **2011**, *50*, 3696.

(48) deKrafft, K. E.; Boyle, W. S.; Burk, L. M.; Zhou, O. Z.; Lin, W. *J. Mater. Chem.* **2012**, *22*, 18139.

(49) Taylor, K. M. L.; Rieter, W. J.; Lin, W. *J. Am. Chem. Soc.* **2008**, *130*, 14358.

(50) Rieter, W. J.; Taylor, K. M. L.; An, H. Y.; Lin, W. L.; Lin, W. B. *J Am Chem Soc* **2006**, *128*, 9024.

(51) Guo, S.; Wang, Y.; Miao, L.; Xu, Z.; Lin, C. M.; Zhang, Y.; Huang, L. *ACS Nano* **2013**, *7*, 9896.

(52) Li, J.; Chen, Y.-C.; Tseng, Y.-C.; Mozumdar, S.; Huang, L. *J. Controlled Release* **2010**, *142*, 416.

(53) Ashley, C. E.; Carnes, E. C.; Phillips, G. K.; Padilla, D.; Durfee, P. N.; Brown, P. A.; Hanna, T. N.; Liu, J.; Phillips, B.; Carter, M. B.; Carroll, N. J.; Jiang, X.; Dunphy, D. R.; Willman, C. L.; Petsev, D. N.; Evans, D. G.; Parikh, A. N.; Chackerian, B.; Wharton, W.; Peabody, D. S.; Brinker, C. J. *Nat. Mater.* **2011**, *10*, 389.

(54) Liu, J.; Jiang, X.; Ashley, C.; Brinker, C. J. *J. Am. Chem. Soc.* **2009**, *131*, 7567.

(55) John, C. S.; Vilner, B. J.; Geyer, B. C.; Moody, T.; Bowen, W. D. *Cancer Res.* **1999**, *59*, 4578.

(56) Banerjee, R.; Tyagi, P.; Li, S.; Huang, L. *Int.J. Cancer* **2004**, *112*, 693.

(57) Aydar, E.; Palmer, C. P.; Djamgoz, M. B. A. *Cancer Res.* **2004**, *64*, 5029.

(58) Park, J.; An, K. J.; Hwang, Y. S.; Park, J. G.; Noh, H. J.; Kim, J. Y.; Park, J. H.; Hwang, N. M.; Hyeon, T. *Nat Mater* **2004**, *3*, 891.

(59) Huang, C. C.; Khu, N. H.; Yeh, C. S. *Biomaterials* **2010**, *31*, 4073.

(60) Baek, M. J.; Park, J. Y.; Xu, W.; Kattel, K.; Kim, H. G.; Lee, E. J.; Patel, A. K.; Lee, J. J.; Chang, Y.; Kim, T. J.; Bae, J. E.; Chae, K. S.; Lee, G. H. *ACS Appl Mater Interfaces* **2010**, *2*, 2949.

(61) An, K.; Kwon, S. G.; Park, M.; Bin Na, H.; Baik, S. I.; Yu, J. H.; Kim, D.; Son, J. S.; Kim, Y. W.; Song, I. C.; Moon, W. K.; Park, H. M.; Hyeon, T. *Nano Lett* **2008**, *8*, 4252.

(62) Pan, D.; Caruthers, S. D.; Hu, G.; Senpan, A.; Scott, M. J.; Gaffney, P. J.; Wickline, S. A.; Lanza, G. M. *J Am Chem Soc* **2008**, *130*, 9186.

(63) Pan, D. P. J.; Senpan, A.; Caruthers, S. D.; Williams, T. A.; Scott, M. J.; Gaffney, P. J.; Wickline, S. A.; Lanza, G. M. *Chem Commun* **2009**, 3234.

(64) Tu, C. Q.; Ma, X. C.; Pantazis, P.; Kauzlarich, S. M.; Louie, A. Y. *J Am Chem Soc* **2010**, *132*, 2016.

(65) Taylor-Pashow, K. M. L.; Della Rocca, J.; Xie, Z. G.; Tran, S.; Lin, W. B. *J Am Chem Soc* **2009**, *131*, 14261.

TOC Graphic:

Mn-zoledronate NCP carries 63 wt% of zoledronate for cancer therapy and 13.3 wt% of Mn^{2+} for T_1-weighted magnetic resonance imaging.